This manuscript was accepted by Phys. Plasmas. Click here to see the version of record.

Statistical Properties of Intermittent Bursts in the Texas Helimak

F. A. C. Pereira,[1] I. M. Sokolov,[2] D. L. Toufen,[3] Z. O. Guimarães-Filho,[1] I. L. Caldas,[1] and K. W. Gentle[4]

[1)] *Institute of Physics, University of São Paulo, 05315-970 São Paulo, São Paulo, Brazil.*

[2)] *Institut für Physik, Humboldt-Universität zu Berlin, D-12489 Berlin, Germany*

[3)] *Federal Institute of Education, Science and Technology of São Paulo, 07115-000 Guarulhos, São Paulo, Brazil.*

[4)] *Department of Physics and Institute for Fusion Studies, The University of Texas at Austin, 78712 Austin, Texas , USA.*

We present investigations of intermittent turbulence in the Texas Helimak, a simple toroidal plasma device in which the turbulence properties are modified by applying a bias voltage. The analyzed turbulence presents high density bursts, detected by Langmuir probes measuring ion saturation current fluctuations. The turbulent time series is reproduced by a synthetic signal model that has bursts with the same temporal profile and random amplitudes, plus a low amplitude fluctuating stochastic background. Using this model, we identify two burst regimes, observed according to the radial position and external bias: in the first regime, the bursts occur in random instants, leading to a Poisson distribution of the time interval between bursts, while in the second regime, the time interval between large bursts are correlated and modeled by a Gamma distribution. Furthermore, we use the shape parameter k, that measures the correlation between occurrence times of successive bursts, to characterize the burst regime in most of the low field side. We find that in the region described by the second regime, the k values increases with positive applied bias.

I. INTRODUCTION

The turbulence in the plasma edge of magnetically confined devices presents intermittent high density peaks[1–4]. These peaks, also called bursts, are associated with coherent structures that are responsible for a important part of the particle and energy transport[5], so they have a strong consequence to the plasma confinement. The bursts present in the scrape-off layer of fusion machines seem to have an universal feature in the plasmas, being also present in other types of magnetically confined plasma machines[6–9].

The bursts presence has been associated with many turbulence properties common to several devices, suggesting universality of convective transport[1]. The convective nature of such structures have been extensive studied on tokamaks[10], and evidences suggest they have similar behavior on helimaks[8,9,11]. The structures can be detected in the far SOL of tokamaks using electrostatic probes, what means that a better understanding of these structures can lead to the possibility of evaluate the plasma performance from SOL probe data.

Several models have been proposed to explain the intermittent turbulence in magnetic confined devices. The turbulence driven energy is associated to universal instabilities[12] and recurrence properties are used to characterize the fluctuation[13]. Recently, a stochastic model was proposed to describe the density time series in the tokamak SOL. In this model, the signal consists of a series of intermittent structures with amplitudes following an exponential probability density function that occur at random instants[14]. It was showed that this model presents a parabolic relation between the signal skewness and kurtosis. This model was compared to gas puff measurements on the Alcator C-Mod and it explains both the density histogram and power spectrum[15].

Besides these relevant results, the burst statistics have not yet been completed determined. As the plasma turbulence in Texas Helimak is similar to those in the tokamak scrape-off layer, the study of the Helimak turbulence supports the effort to elucidate the tokamak turbulence. This, allied with the possibility of measuring bursts at several positions in Texas Helimak and control its statistics by applying a electrostatic bias voltage, opens a possibility to complement the mentioned previous results.

In this work, we study the turbulence in low-field side region of the Texas Helimak[16] using the data from a set of Langmuir probes present in the machine. This turbulence presents extreme events that consist of bursts with density much larger than the average.

The number of extreme events and the turbulence level can be modified in this machine by imposing an electrostatic bias voltage in the plasma[8,11].

We use the model of bursts train turbulence[14] to describe the intermittent turbulence. We identify two different intermittent regimes that occur in different parts of the machine low field side. One regime, found on the region closer to the density maximum and with large radial density gradient, is similar to the regime found on scrape-off layer of tokamaks, and it can be described as large uncorrelated and randomly occurring bursts plus small density background with colored Gaussian distribution. A second regime was found further in the low field side, in the region with small gradient, that cannot be described by a model with uncorrelated bursts occurrence times. We found that the turbulence consists mostly of large bursts with correlated occurring instants but uncorrelated amplitudes, and this instant correlation is seen as a broad peak in the power spectrum.

In section II we introduce the Texas Helimak and present its main characteristics. In section III we present the properties of the turbulent signal for two selected radial positions of the Texas Helimak and apply the model for the two selected regions. In section IV, we apply the model in a large interval of radial positions. A summary of the results focused on the similarities and differences observed in the turbulence regimes of these regions is presented in section V.

II. THE TEXAS HELIMAK

The Texas Helimak[16] is a basic plasma machine with toroidal vessel and open helical magnetic field lines having a large toroidal component and very small vertical component. It presents an one-dimensional magnetohydrodynamic equilibrium, depending basically only on the radial position R. The machine presents magnetic curvature and shear and also flow shear as in the tokamak plasma edge and SOL.

The Texas Helimak has a large array of Langmuir probes, located on 16 plates present at the machine top and bottom and a data acquisition system that can collect data from 96 probes simultaneously at 500 ksamples/s for 10 seconds[17]. It is possible to impose a common electrostatic potential (bias) on the plates colored in figure 1(a) to change the electrostatic field radial profile and electrostatic modes. With this biasing, we investigate the influence of the electric field profile on the turbulence and transport. The data used in this analysis are

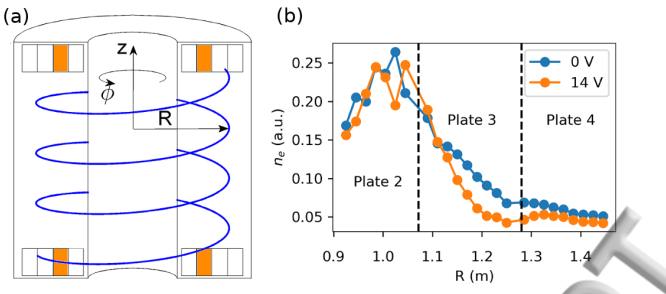

FIG. 1. (a) Texas Helimak vacuum chamber showing an example of the magnetic field lines and the plates used as a support for the Langmuir probes. (b) Density profiles for two different biasing potentials.

ion saturation current signals measured in a large number of radial positions in the whole machine and in a rectangular grids of probes mounted on specific plates.

III. STATISTICAL DESCRIPTION OF TURBULENCE

As usual, for the turbulence analysis, we introduce the normalized ion saturation current signal:

$$\Phi(t) = \frac{I_s(t) - \langle I_s \rangle}{\sigma_I} \tag{1}$$

where $\langle I_s \rangle$ is the time average of the ion saturation current I_s and σ_I is the standard deviation. In low field side, the ion saturation fluctuation distribution presents an exponential tail. The turbulence can be suppressed when a negative potential is applied on the plate where the density maximum is located (plate 2 in Fig. 1(b)), what eliminates the intermittency and reduces the turbulence level[16].

On the other hand, the intermittent turbulence can be enhanced when a positive bias is applied[8]. The biasing increases the number of bursts and their amplitudes. As we are interested on studying the bursts dynamics, the positively biased case was used. Figure 2 shows two examples of ion saturation turbulent signal for two different positions of the machine low-field side: a position with a large radial density gradient ($R = 1.11$m) and a position where the density is almost constant ($R = 1.25$m), but still close to the gradient (and electrostatic bias) region.

In both cases, the time series (Fig. 2(a)), presents many high density bursts, where the

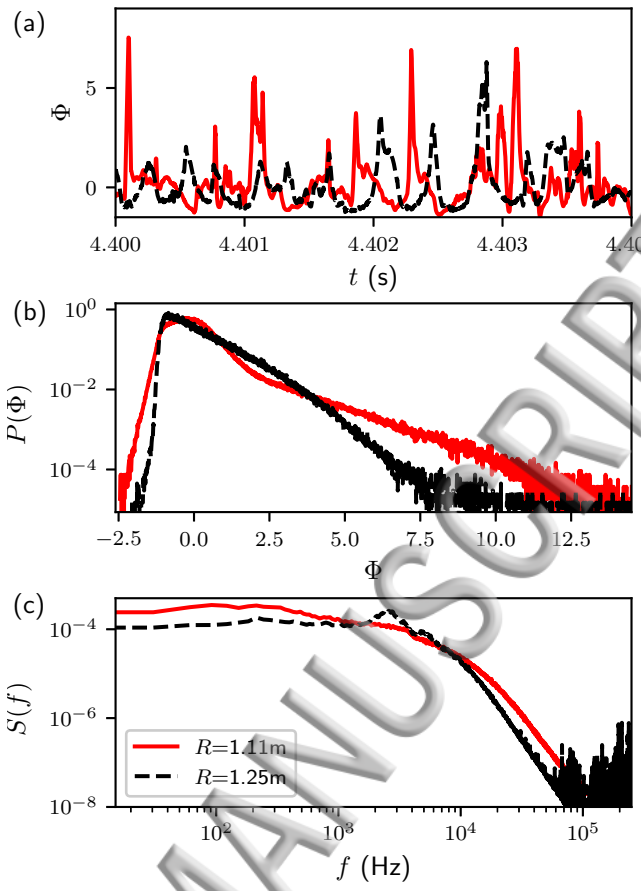

FIG. 2. Example of normalized ion saturation current time series (a), signal histogram (b) and power spectrum (c) for the two considered positions ($R = 1.11$m and $R = 1.25$m).

signal achieves many standard deviations above average. The presence of bursts is reflected on the signals histograms (Fig. 2(b)) as they have exponential tails for large density fluctuation amplitudes. The density bursts are also reflected in the power spectrum (Fig. 2(c)), as the power spectra present a low frequency plateau and power law decay for high frequency, a similar situation as found in the scrape-off layer of tokamaks[15]. The plateau and tail are associated with the interburst dynamics and individual burst temporal profile, respectively. While the presence of bursts makes the turbulence in both positions similar, a more careful investigation shows an interesting difference:the radial position of $R = 1.25$ m present a broad peak in the power spectrum (Fig. 2(c)) for a frequency around 3 kHz.

For the bursts statistics, we defined a burst as a local maximum at least two standard deviations above the signal average. With this threshold, one Texas Helimak shot have about ten thousand bursts. Thresholds above two standard deviations have almost no effect on the

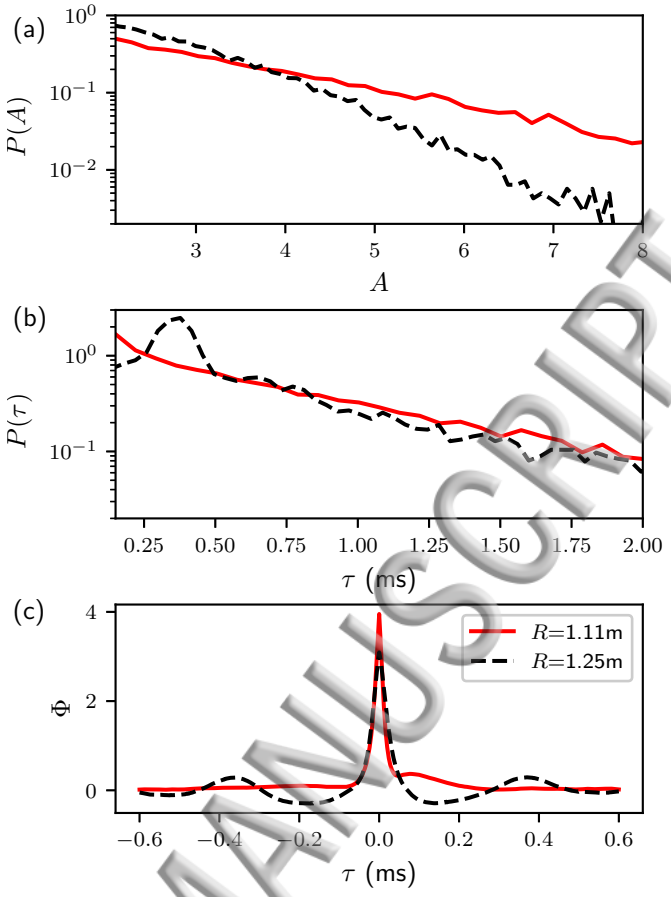

FIG. 3. Histogram of bursts amplitude (a), times between bursts (b) and burst conditional average (c)for the two considered positions (R = 1.11m and R = 1.25m), for a burst threshold of two standard deviations above average.

conditional average burst profile, except for the expected relationship between the average peak amplitude and the threshold value. The bursts amplitudes in both cases (Fig. 3(a)) follow exponential distributions, as observed in other magnetic confined plasma devices[18,19]. The waiting times distributions (Fig. 3(b)) have different characteristics: for the R=1.11 m position, we have Poisson process exponential, as identified in other machines; but at the R=1.25 m position, the histrogram shows a maximum at 0.35 ms, clearly deviating from the exponential profile.

In Figure 3(c), we present the conditional average for both cases. For times close to the burst maximum both cases have a similar exponential increase and decay. In the signal measured at R = 1.11 m, the bursts return fast to the average value, but in the signal measured at R = 1.25 m, there is an oscillation before and after the main burst maximum.

Even more, this oscillation frequency matches the peak frequency from the power spectrum, suggesting that both are evidences of the same process.

The turbulence signal measured at $R = 1.11$ m present many features already found in scrape-off layer of tokamaks, so it can be modeled in the same way with small adaptations. But the signal measured at $R = 1.25$ m presents a striking difference: it shows a characteristic time that appears in the power spectrum, burst awaiting times and conditional average. A model must be able recover the characteristic time in these three measurements simultaneously to be deemed adequate.

A. Random Arrival Time Burst Regime

When we apply the standard burst model (appendix A) to describe the turbulence in the Texas Helimak, it is not possible to fit simultaneously the bulk of the signal histogram and the exponential tail. This impossibility can be seen in Figure 4(a), where the histogram of the simulation with only burst (continuous blue line) and the experimental data (red dotted line) are shown, in which the exponential tail is well reproduced but the region of negative Φ is not well described.

We addressed this issue by inserting a background noise component $n_b(t)$ in the signal model:

$$n(t) = \sum_j A_j g(t - t_j) + n_b(t)\,, \tag{2}$$

to fit the bulk of the distribution and density average value. In this case, we considered the n_b as an Gaussian colored noise process ($S \propto f^{-1.3}$). This extra term make sense as we are analyzing a position close to the density maximum, where local plasma generation and diffusive transport can make significant contribution to the total plasma content. In figure 4, we show in green dashed lines the histogram, power spectrum and burst conditional average of the simulated signal, that matches fairly well the experimental data at $R = 1.11$m. The green line obtained by applying Eq. 2 fits well the experimental data.

As the model describes well the experimental data, we applied it for some bias values, so we can calculate the effect of increasing the bias on the turbulence properties. Figure 5 shows the effect of the bias on three turbulence model parameters, obtained from the fitting procedure of the experimental data: the burst rate, the mean burst amplitude $\langle A \rangle$ and the

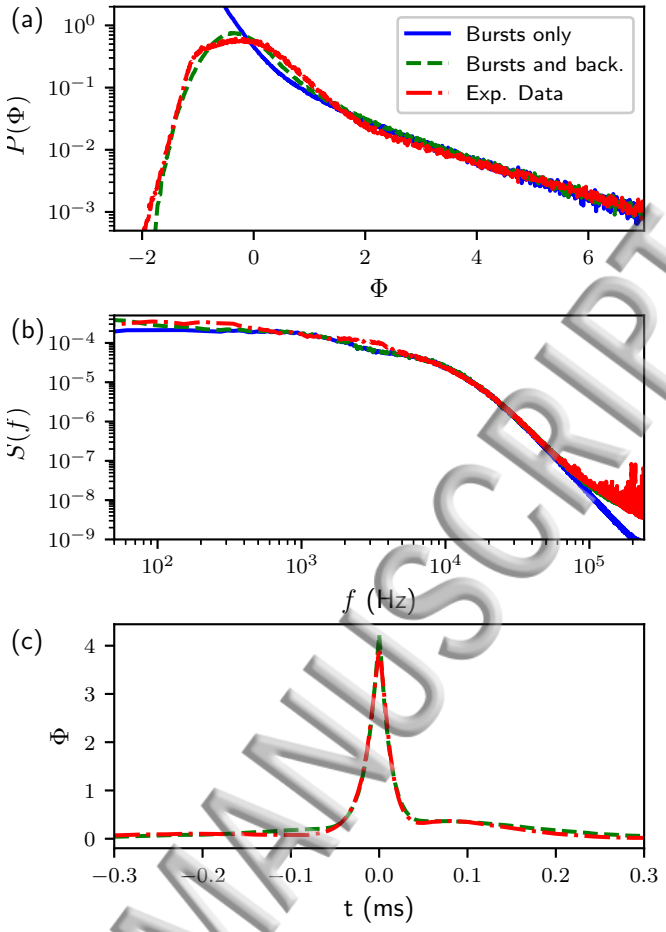

FIG. 4. Signal histogram (a), power spectrum (b) and burst conditional average of the density gradient region (red), compared with the model with only the bursts (blue line) and with bursts plus background (green dashed),

background standard deviation σ_b. One important feature of this model is that the burst detection using a threshold is only a reliable measure of burst count if the time between bursts is much larger than the burst duration[20]. Therefore the fitted burst rate is a more reliable estimate than the number of peaks above a threshold, as the increase in burst numbers also increase signal average and standard deviation, a complex interaction that lead to underestimating the burst rate by a factor that grows with the burst rate.

Earlier analysis of the burst rate in the region of the Texas Helimak[8] considered in this section, using threshold detection showed similar trend on the burst rate we observe with the model fitting (Fig. 5(a)), but with a burst rate more than one order of magnitude smaller, as the lower amplitude bursts were cut out. The model fitting shows an interesting feature:

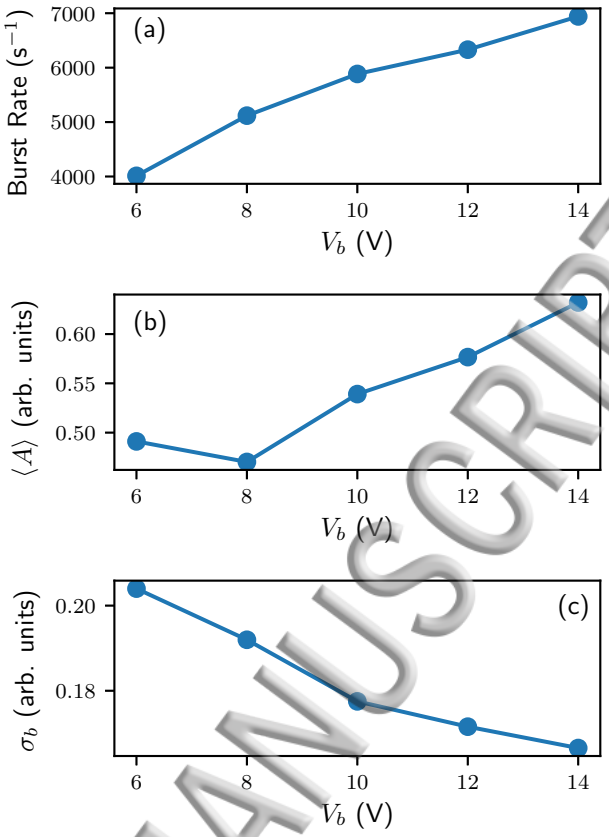

FIG. 5. Burst rate (a), amplitude (b), and background standard deviation (c) obtained from fitting the time series model for positive bias values.

the burst amplitude (Fig. 5(b)) increases with the bias, while the background fluctuation (Fig. 5(c)) is decreasing. So the biasing not only increases the number of bursts, increasing the intermittent turbulence, but also reduces the background turbulence.

It is interesting to point out that, in this position, the intermittent turbulence (bursts) is suppressed by applying a negative bias[11]. The suppression and the trend for positive biases make us conclude that the bursts are actually mounted on a background Gaussian turbulence that dominates when we suppress the bursts.

B. Renewal Process Burst Regime

Three important features in the signal measured at $R = 1.25$ m make it different from the signal considered in the previous section on a first look: a peak on the power spectrum, an

oscillation found at the conditional average and a peak in the burst waiting time histogram. These three features also have matching frequencies. This fact alone is enough to question the random burst arrival time hypothesis.

While the power spectrum peak may arise from a purely background oscillation (as opposition of a burst characteristic waiting time), if the bursts are independent of the background, they would happen at random phases of the background oscillation. The conditional analysis would average out the oscillation, except for a secondary effect of bursts being more likely to be detected at the oscillation crest. The same argument holds for the measured waiting time histogram, and the deviation from a exponential waiting time would be too small. So the burst conditional average and waiting time histogram indicate that the process responsible for the power spectrum peak is related to the bursts dynamics.

A simple way to insert a characteristic time in the bursts waiting times is to describe the burst appearance as a renewal process[21,22]. This way, the waiting time distribution between two consecutive bursts becomes an arbitrary function $\rho(\tau)$, that is the same for all bursts and only depends on the waiting time interval τ. When the distribution ρ is an exponential function, we recover the Poisson process.

If we consider that the bursts have amplitudes with average A_0, variance σ_A^2 and that an individual amplitude is independent of waiting times and previous amplitudes, we can write the power spectrum as:

$$S(\omega) = |G(\omega)|^2 \frac{A_0^2}{\tau_0} \left(\frac{\sigma_A^2}{A_0^2} + \frac{1 - |\hat{\rho}(\omega)|^2}{|1 - \hat{\rho}(\omega)|^2} \right) , \tag{3}$$

where $S(\omega)$ is the power spectrum, and $\hat{\rho}$ is the one-sided Fourier transform of the waiting time distribution ρ. An estimation of ρ directly from the experimental power spectrum is an ill-posed problem. We consider that the waiting times distribution follows a family of functions with a small number of parameters. We adopt a gamma distribution:

$$\rho(\tau; k, s) = \frac{\tau^{k-1} e^{-\frac{\tau}{s}}}{\Gamma(k) s^k} , \tag{4}$$

where k and s are the shape and scale parameters. We choose this distribution because it has interesting features: the shape parameter k is equal to $(\bar{\tau}/\sigma)^2$ and when it is $k = 1$, we recover the Poisson process; the parameter s is responsible for the scale, as $\bar{\tau} = ks$; it is infinitely divisible and a rather common distribution for time intervals modeling.

We estimate the burst characteristic shape by fitting the burst conditional average. We eliminate the oscillation by separating the below zero intervals in the Φ time series, shuffling them and reinserting at the new order, creating a new time series. Then, we fit the conditional average of the new series.

The last ingredient for fitting is the amplitude standard-deviation over its average. For that, we defined a really low threshold (a fraction of the standard deviation above the signal average), a small burst detection dead time (below the shape characteristic time τ_0) and estimated its distribution from the amplitudes histogram.

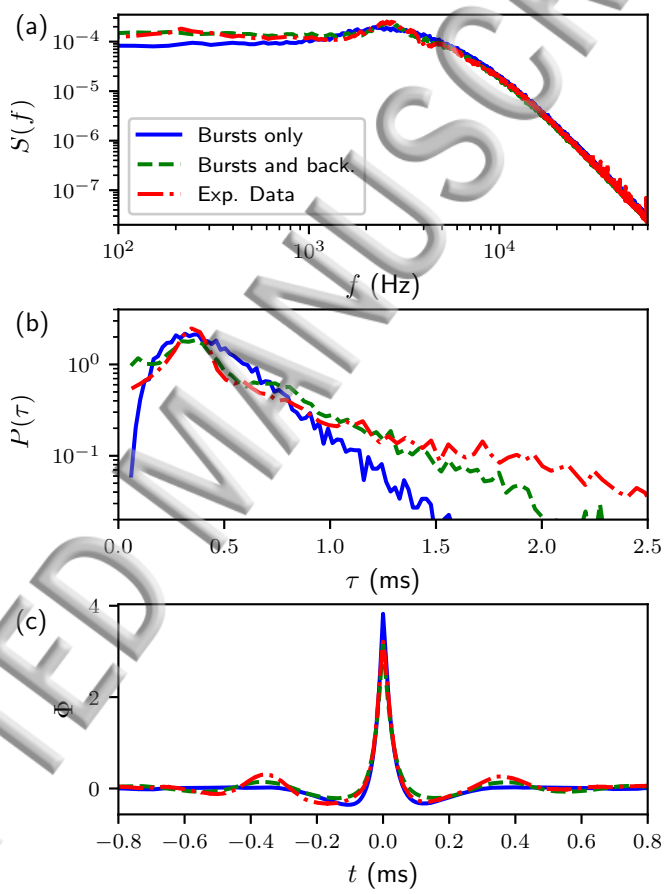

FIG. 6. Power spectrum (a), waiting times histogram (b) and detected bursts conditional average for a simulation with bursts and background.

After that, we did a non-linear least-squares fitting of equation 3, using the Fourier transforms of the burst shape and waiting times distribution obtained analytically. Figure 6 shows the experimental and bursts-only fitted results. The qualitative features of the power spectrum (Fig. 6(a)) and the burst conditional average (Fig. 6(c)) are recovered, but we got

a burst waiting time distribution that has a broader top and a shorter tail. The tanoil decay of the detected waiting time distribution is very sensitive to the series average and standard deviation, because its expected value and the burst count are directly related.

Figure 7 shows the histograms of Φ for the time series and the bursts-only simulation. As we found for the previous case (Fig. 4), the bursts-only time series fails to recover the experimental fluctuation distribution. In the data considered here, the experimental histogram is similar to a gamma function that arises from the original burst train model[14,15]. But the burst rate is defined by the characteristic frequency observed from the conditional average, power spectrum and burst waiting time.

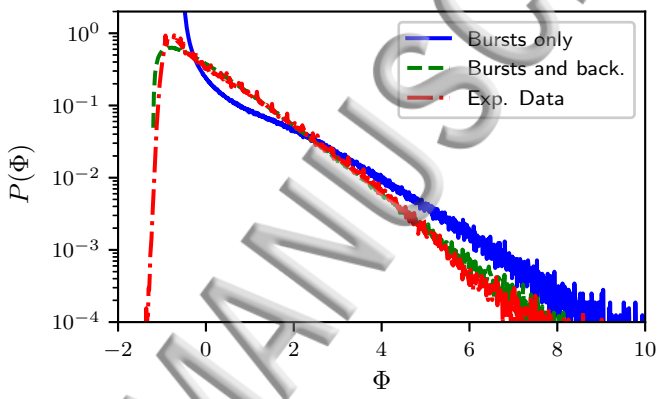

FIG. 7. Histograms of the simulation with only the correlated bursts, with bursts and background and of the experimental data.

One way to work around these two apparently conflicting evidences, burst rate from characteristic frequency versus from the signal histogram, is to consider the time series is made from the sum of two burst time series: a large bursts that follow a renewal process, and a random background bursts. The background bursts do not have a peak frequency, as they are uncorrelated (with exponential amplitude distribution), and share the same shape as the main ones. A background that is composed by small bursts may be seem as these bursts are from an inner position (where they are completely uncorrelated) and were attenuated by the parallel losses during their propagation.

The figures 6 and 7 also show the results of the correlated large bursts and uncorrelated (background) bursts simulation. The power spectrum (Fig. 6(a)) is better represented by the new simulation as the background presence increases the low frequency plateau. The detected burst waiting times (Fig. 6(b)), is well recovered in this simulation, with a slightly

faster decay, which indicates a higher burst count in the simulation. The burst conditional average (Fig. 6(c)) is also well reproduced, what indicates that the oscillation is indeed an effect of the burst waiting time probability distribution and not an individual burst feature.

The simulated histogram also recovers the experimental one nicely (Fig. 7), with small differences close to the histograms maxima and at the high density tails. The differences at the high density tail is probably related to the waiting time tails: in the simulation, large density values (bursts) are more probable, what increases the number of bursts and this makes the tail of detected waiting times distribution decrease faster.

IV. RADIAL AND BIAS DEPENDENCE

So far, we presented a detailed study of two different turbulence regimes that are well described by a model that consists of a burst train plus a background. Now, we can extend this analysis for a large radial region on the low field side, so we can get the whole picture of the burst regime in this region. The most important features fo help understanding the radial dependence of the burst train, and to look for connections on the burst process on different regions are the presence of peaks on the power spectrum and the bursts waiting time shape parameter k (responsible for the intensity of the subsequent burst times correlation). While the first feature is straightforward, obtaining the second from the power spectrum is very error prone when the background is not adequately estimated. We solved this issue by estimating k directly from the waiting time histograms, as the large bursts are mostly unaffected by the background.

Figure 8(a) shows how the power spectrum changes with the radial position. In the density peak and most of the gradient region, the power spectrum presents no peak in the kHz region, as observed in the $R = 1.11$ m probe data that was analyzed in section III A. From $R = 1.15$ m on, a broad peak between $f = 3.5$ kHz and $f = 1.5$ kHz appears, with the relative amplitude increasing as the radius increases and its frequency decreases. In Fig. 6 we showed that, in $R = 1.25$ m, this peak can be understood as consequence of the correlation between successive bursts arrival times and it was modeled by a renewal process on the burst occurrence instants.

The radial dependency of the peak frequency, that is associated (at least on plate 3) to the bursts waiting time process, suggests that bursts must be formed locally and do not come

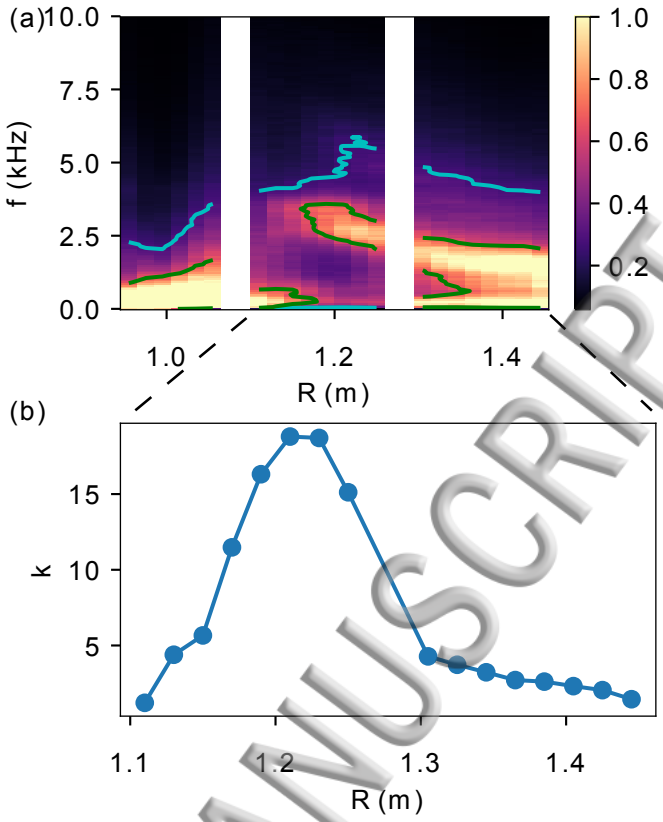

FIG. 8. Normalized signal power spectrum for the whole radial range (a), and radial dependence of the shape parameter for the renewal process estimated from the burst waiting time distributions (b).

from a much more internal position. This result is in agreement with the burst propagation parameters for the Texas Helimak estimated in Ref.[11], where the bursts propagation and shape parameters indicate that they do not propagate further than few centimeters in the radial direction.

In Figure 8(b) we show the shape parameter k obtained from the fitted waiting time distributions (see appendix C); this parameter indicates how much the burst process deviates from an uncorrelated random process, as $k = 1$ recovers a Poisson process and $k \gg 1$ indicates a well defined time between subsequent bursts. This figure shows clearly the two different regimes presented and the transition between them: the Poisson like regime of the more internal region ($R = 1.11$ m) and renewal process regime (from $R = 1.19$ to 1.25 m). The far low field site presents a third scenario ($R = 1.3$ to 1.45 m), in which the occurrence time correlation is weak and cannot be the only responsible for the peak in the spectrogram.

Therefore, the 2 kHz peak observed in the signal measured at this region is mainly due to the background oscillation.

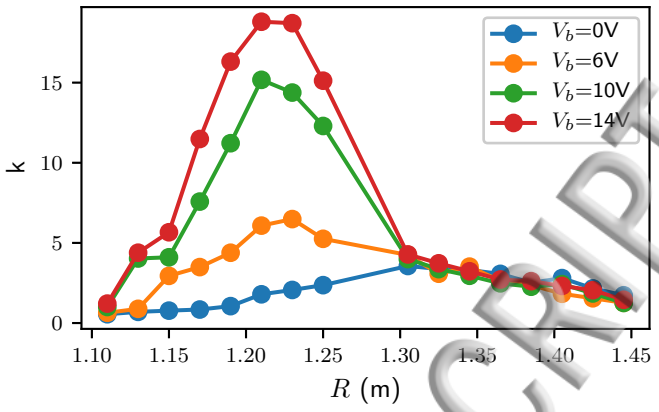

FIG. 9. Radial dependence of the burst waiting time shape parameter k for four different electrostatic bias values.

Figure 9 shows the electrostatic bias effect on bursts waiting time parameter k. The bias has almost no effect far from the applied region (plate 4), in agreement with other turbulence properties analyzed in a previous work[11], where it was found that the burst propagation and shape parameters are not changed by the bias in this region. Closer to the electrostatic bias applied region (plate 3), it is already known that positive biasing increases the burst count[8] and affects significantly the bursts shape and propagation properties[11]. The biasing effect on the waiting time distribution is consistent with this picture, as we can see the appearance of a preferred inter-burst time interval as the bias is increased, a time interval that is reflected on the power spectrum as a peak around 3 kHz.

V. CONCLUSION

We investigated the bias enhanced intermittent turbulence in the Texas Helimak. This turbulence presents high density bursts, much larger than the average density. We showed that the intermittent turbulence has different regimes. We described two regimes by considering the turbulence as composed mainly by a sum of bursts with same temporal profile and random amplitudes. We showed that the power spectrum power law decay is a consequence of the temporal profile of the individual bursts.

We showed that, in a position close closer to the density maximum, the turbulent signal

can be described by a sum of Gaussian background and randomly occurring bursts with amplitudes following an exponential distribution. This regime is very similar to observed in the SOL of tokamaks[15], with the differences being only the existence of background oscillation and a small correction on the burst profile. As this position is close to the density maximum, the background can be understood as a consequence of diffusion or local plasma generation. The model allowed us to better characterize the effect of biasing and conclude that increasing the bias potential has a double effect: it decreases the background turbulence and increases the burst rate and amplitude.

In the position at a larger radius, at the beginning of a region with relatively constant density ($R = 1.25$ m), we found that bursts do not appear at random instants, as their occurrence times depend on when the last burst appeared. We showed that turbulence properties in this region are well described by a model in which the large bursts follow a renewal process with random amplitudes. This model is enough to describe the power spectrum, the maximum observed in the bursts waiting time distribution and the oscillation in burst conditional average. We fitted the experimental signal histograms by adding a background with small uncorrelated bursts.

After presenting these two turbulence regimes, we analyzed the burst regime in a large interval of the low field side. We characterized the burst dynamics according to shape parameter k of the waiting time distribution by fitting the experimental waiting time histograms. We found that the power spectrum frequency peaks appears in a region with large k values. This region also presents a clear radial dependence of the peak frequency (and characteristic waiting time), what indicates that the large and time-correlated bursts must be formed locally. We also analyzed the radial profile for many bias voltages and found that in the large k region the burst correlation is driven by the electrostatic biasing, as the k values increases with the bias value.

Further on the low field side, the frequency peak persists, but the parameter k values indicates that the bursts waiting time correlations are not strong enough to generate it, so the power spectrum peaks are probably a consequence of background oscillations. This region is also far from the position where the bias is applied and are not affected by it, a result that is consistent with previous works that analyzed the burst propagation parameters[11].

This manuscript was accepted by Phys. Plasmas. Click here to see the version of record.

ACKNOWLEDGMENTS

We would like to thank this work financial support by the Brazilian agencies São Paulo Research Foundation (FAPESP) - grants 2014/07043-0, 2015/50122-0, 2017/23128-3 and 2018/03211-6 - and CNPq - grant 141192/2016-0.

Appendix A: Bursty Time Series Model

It was proposed that many properties of tokamaks SOL can be described by supposing that the plasma there consists only of high density bursts with a characteristic shape, occurring at random instants with amplitudes randomly sampled from an exponential distribution[14,15,19]. In this model, we can write the electron density time series as

$$n_e(t) = \sum_j A_j g(t - t_j)\,, \tag{A1}$$

where $g(t)$ is the burst shape function, A_j and t_j are the burst amplitudes and arrival time. In this model, the power spectrum of the signal can be written simply as:

$$S(\omega) = |G(\omega)|^2 R(\omega)\,, \tag{A2}$$

where $G(\omega) = \mathcal{F}[g(t)]$ is the Fourier transform of an individual burst shape and $R(\omega)$ is the power spectrum of the (stochastic) process associated with arrival times t_j and amplitude A_j. When the bursts have independent amplitudes A_j and times t_j, $R(\omega) = \langle A^2\rangle/\langle\tau\rangle$, where $\langle\tau\rangle$ is the average time between two consecutive bursts. To estimate $g(t)$, we considered that the burst conditional average profile reflects the typical burst shape, multiplied by a constant. Then we used non-linear least-squares to fit the shape function $g(t)$:

$$g(t) = e^{-|t|/t_0} + ae^{-\frac{(t-t_g)^2}{2s_t^2}} \tag{A3}$$

where $t_0 = \lambda t_d$ for $t \geq 0$ and $t_0 = (1-\lambda)t_d$ for $t < 0$, t_d is the burst characteristic time, a is the amplitude of a small Gaussian correction, t_g and s_t are the Gaussian correction location and width, respectively. This function is similar to the one employed in other works[14,15]. The main difference here is the small Gaussian term used to fit the small bump just after the burst, visible in the conditional average for $R = 1.11m$ (Fig. 3(c)).

This manuscript was accepted by Phys. Plasmas. Click here to see the version of record.

Appendix B: Background Model for $R = 1.25$ m

If the background oscillations and the burst generation process are independent, the power spectral density can be written as:

$$S_{new}(\omega) = S(\omega) + S_b(\omega)\,, \tag{B1}$$

where $S(\omega)$ is given from eq. A2 and $S_b(\omega)$ is the background power spectral density. With the hypothesis of bursts as a background, the shape of high frequency power decay is guaranteed. Given that the background bursts are uncorrelated, the power spectrum can be expressed as:

$$S_{new}(\omega) = |G(\omega)|^2 \left[\frac{A_0^2}{\tau_b}\left(\frac{\sigma_A^2}{A_0^2} + \frac{1-|\hat{\rho}|^2}{|1-\hat{\rho}|^2}\right) + \frac{A_s^2}{\tau_w}\right] \tag{B2}$$

where τ_b is the average waiting time between bursts, A_s is the mean square amplitude of a background event and τ_w is its average waiting time. We fit the power spectrum expression using non-linear least-squares and iteratively adjusted A_0^2, A_s^2 and τ_w to match the experimental data average and standard deviation.

Appendix C: Waiting Time Fits

The waiting time histograms obtained from threshold detected bursts is a direct way to estimate the inter burst times. But as we have very different bursts amplitudes, it is impossible to be sure that all bursts are detected, specially if we have a non burst-like background oscillation. It is necessary to take the effect of undetected bursts on the waiting time histograms. If we are detecting bursts using a threshold Θ, the probability of a burst be detected α is

$$\alpha(\Theta) = \int_{\Theta}^{\infty} \rho(A) dA\,, \tag{C1}$$

where $\rho(A)$ is the burst amplitude probability density distribution. When the subsequent bursts amplitudes are independent, the detected waiting time p.d.f. $p(\tau)$ needs to take into account the contribution of all possible number of missing bursts. The detected waiting time p.d.f. can be calculated from the real waiting time p.d.f. $\rho(\tau)$ and the burst detection rate α:

$$p(\tau) = \alpha \sum_{j=1}^{\infty} (1-\alpha)^{j-1} \int_0^{\infty} \delta\left(\tau - \sum_{i=1}^{j} t_i\right) \prod_{i=1}^{j} \rho(t_i) dt_i \,. \tag{C2}$$

While this expression is rather complex, the integral is a convolution of j random variables with the same distribution $\rho(t)$, so it can easily expressed in the Laplace or One-sided Fourier domain:

$$P(\omega) = \alpha \sum_{j=1}^{\infty} (1-\alpha)^{j-1} \hat{\rho}(w)^j = \frac{\alpha \hat{\rho}(\omega)}{1-(1-\alpha)\hat{\rho}(\omega)} \,, \tag{C3}$$

where $P(w)$ is the Fourier Transform of the detected waiting time probability density function and $\hat{\rho}(w)$ is the real waiting time p.d.f.. We can substitute the $\rho(\tau)$ from eq. 4:

$$P(\omega) = \frac{\alpha}{(1+i\omega s)^k - (1-\alpha)} \,. \tag{C4}$$

With this expression, obtain a family of detected waiting time distributions $p(\tau; \alpha, k, s)$ by calculating the inverse Fourier Transform of $P(\omega)$. We estimated the waiting time distribution parameters from the experimental histograms using non-linear least-squares method. The $p(\tau)$ was estimated using a fast Fourier Transform with 2^{14} points and subsequent interpolation. Thus, from the analyzed waiting time distribution, we determined the radial profiles of parameter k shown in Figs. 8 and 9.

REFERENCES

[1]G. Y. Antar, S. I. Krasheninnikov, P. Devynck, R. P. Doerner, E. M. Hollmann, J. A. Boedo, S. C. Luckhardt, and R. W. Conn, Phys. Rev. Lett. **87**, 065001 (2001).

[2]S J Zweben , J A Boedo, O Grulke , C Hidalgo, B LaBombard, R J Maqueda, P Scarin and J L Terry, Plasma Phys. Contr. F. **49** S1-S23 (2007).

[3]D. A. D'Ippolito,1, J. R. Myra, and S. J. Zweben, Phys. Plasmas **18**, 060501 (2011).

[4]J. E. Maggs and G. J. Morales, Plasma Phys. and Contr. F. **54**, 124041, 2012.

[5]G. Y. Antar, G. Counsell, Y. Yu, B. Labombard and Pascal Devynck, Phys. Plasmas **10**, 419 (2003).

[6]B. Ph. van Milligen, R. Sánchez, B. A. Carreras, V. E. Lynch, B. LaBombard, M. A. Pedrosa, C. Hidalgo, B. Gonçalves, R. Balbín, and The W7-AS Team, Phys. Plasmas **12**, 052507, 2005.

[7]T. A. Carter, Phys. of Plasmas **13**, 010701, 2006.

[8]D. L. Toufen, F. A. C. Pereira, Z. O. Guimarães-Filho, I. L. Caldas and K. W. Gentle, Phys. Plasmas **21**, 122302 (2014).

[9]I. Furno , B. Labit, A. Fasoli, F. M. Poli, P. Ricci, C. Theiler, S. Brunner, A. Diallo, J. P. Graves, M. Podestà, and S. H. Müller, Phys. Plasmas **15**, 055903 (2008).

[10]S. I. Krasheninnikov, D. A. D'Ippolito and J. R. Myra, J. Plasma Phys. **74**, 679, 2008.

[11]F. A. C. Pereira, D. L. Toufen, Z. O. Guimarães-Filho, I. L. Caldas and K. W. Gentle, Plasma Phys. Contr. F. **58**, 054007 (2016).

[12]I. L. Caldas, H. Tasso, Plasma Physics **20**, 1299 (1978).

[13]M. S. Baptista, M. V. A. P. Heller, I. L. Caldas, 1. A.A. Ferreira, R. Bengtson, J. Stöckel, Phys. of Plasmas **8**, 4455 (2001).

[14]O. E. Garcia, Phys. Rev. Lett. **108**, 265001 (2012).

[15]A. Theodorsen, O.E. Garcia, R. Kube, B. LaBombard and J.L. Terry, Nucl. Fusion **57**, 114004 (2017).

[16]K. W. Gentle e H. Huang, Plasma Sci. and Technol. **10**, 284, 2008.

[17]D. L. Toufen, Z. O. Guimarães-Filho, I. L. Caldas, J. D. Szezech, S. Lopes, R. L. Viana and K. W. Gentle, Phys. Plasmas **20**, 022310, 2013.

[18]R Kube , A Theodorsen, O E Garcia, B LaBombard and J L Terry, Plasmas Phys. Contr. F. **58**, 054001 (2016).

[19]O. E. Garcia, J. Horacek, and R. A. Pitts, Nucl. Fusion **55**, 062002 (2015).

[20]O. E. Garcia, R. Kube, A. Theodorsen, and H. L. Pécseli, Phys. Plasmas **23**, 052308 (2016).

[21]W. Feller, *An Introduction to Probability Theory and Its Applications*, John Wiley & Sons, 2nd Edition, Vol. 2 (1971).

[22]A. V. Holden, *Models of the Stochastic Activity of Neurones*, Springer-Verlag, Berlin (1976).

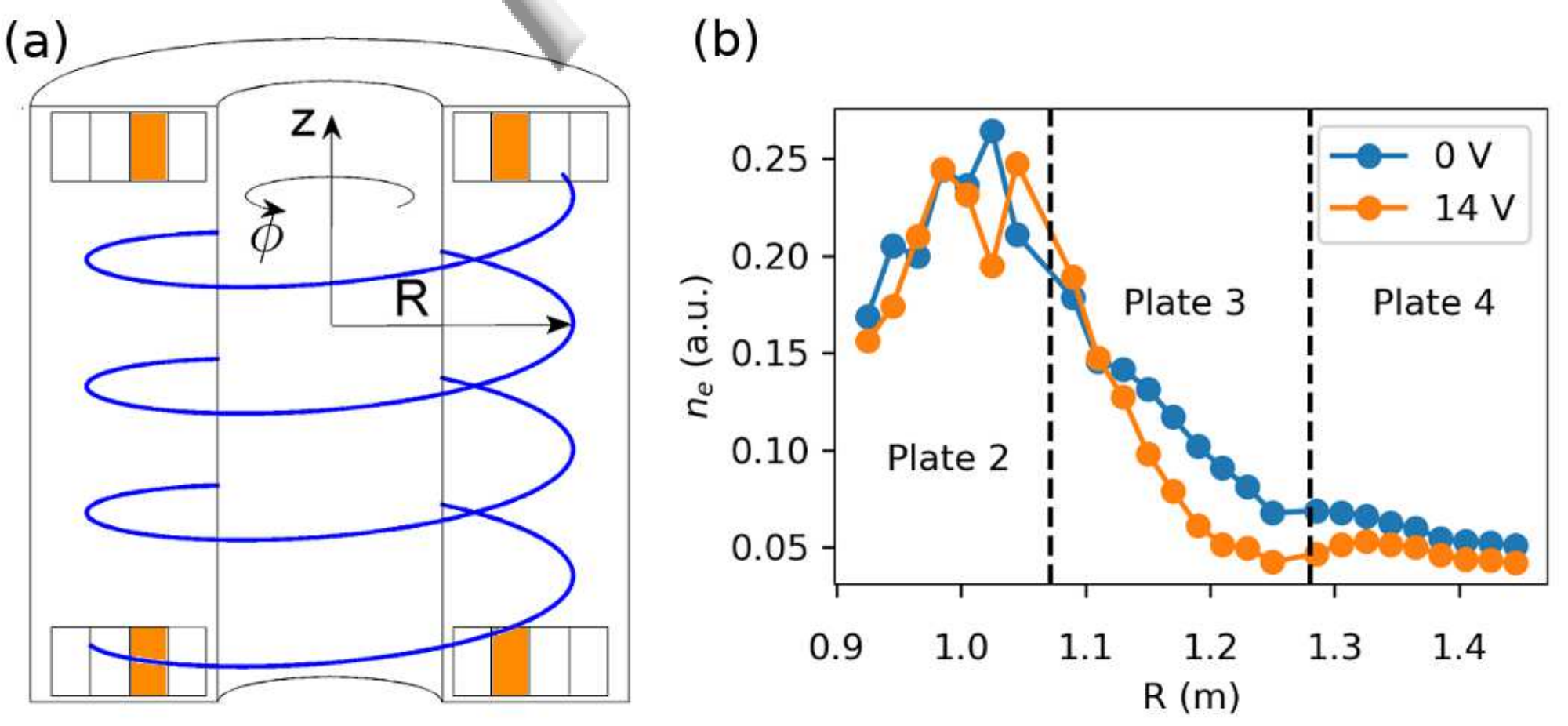
(a)
z
ϕ
R
(b)
0.25
0.20
0.15
0.10
0.05
n_e (a.u.)
Plate 2
Plate 3
Plate 4
0 V
14 V
0.9
1.0
1.1
1.2
1.3
1.4
R (m)

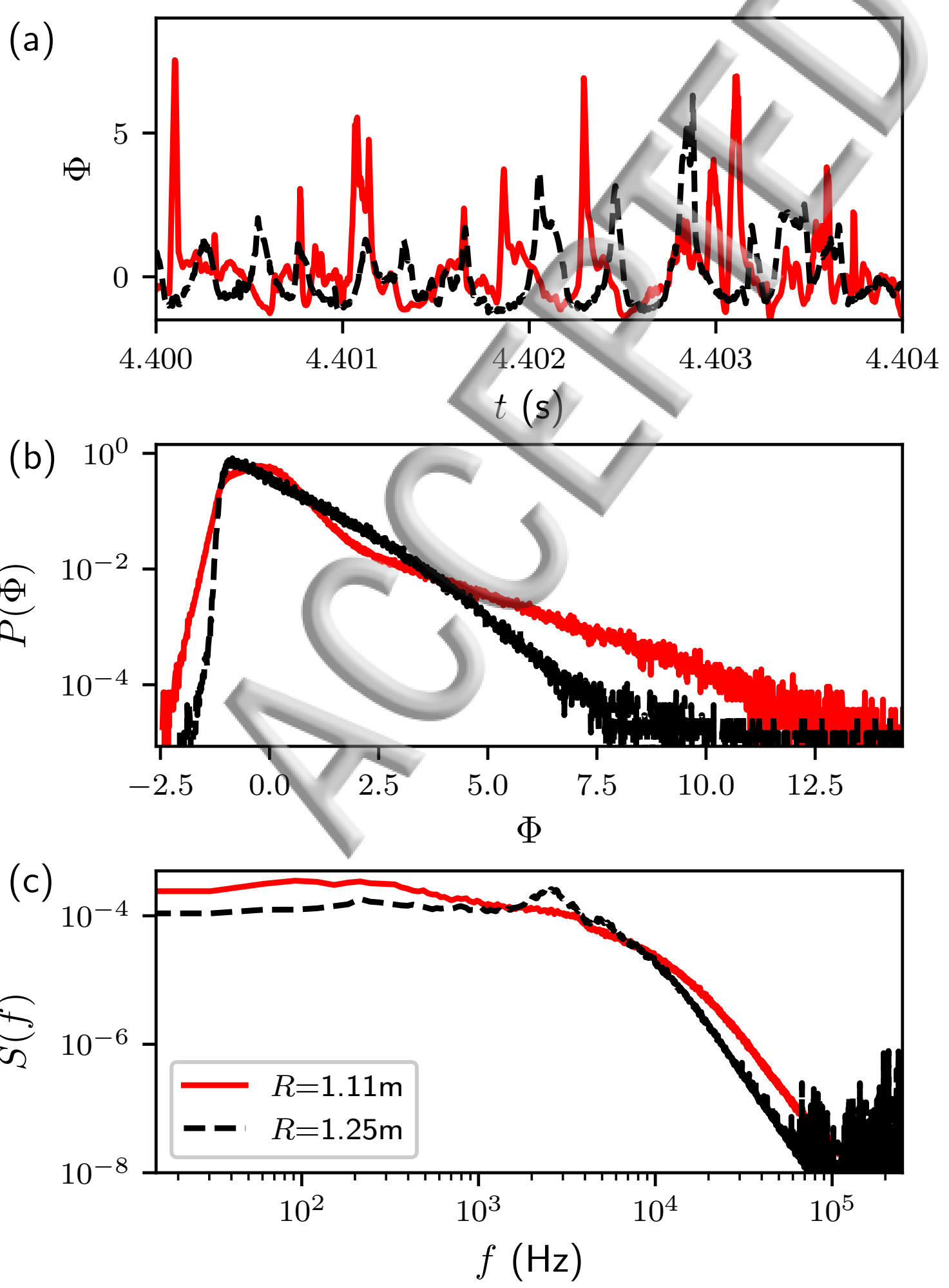
(a)
Φ
5
0
4.400
4.401
4.402
4.403
4.404
t (s)
(b)
10^0
10^−2
10^−4
P(Φ)
−2.5
0.0
2.5
5.0
7.5
10.0
12.5
Φ
(c)
10^−4
10^−6
10^−8
S(f)
R=1.11m
R=1.25m
10^2
10^3
10^4
10^5
f (Hz)

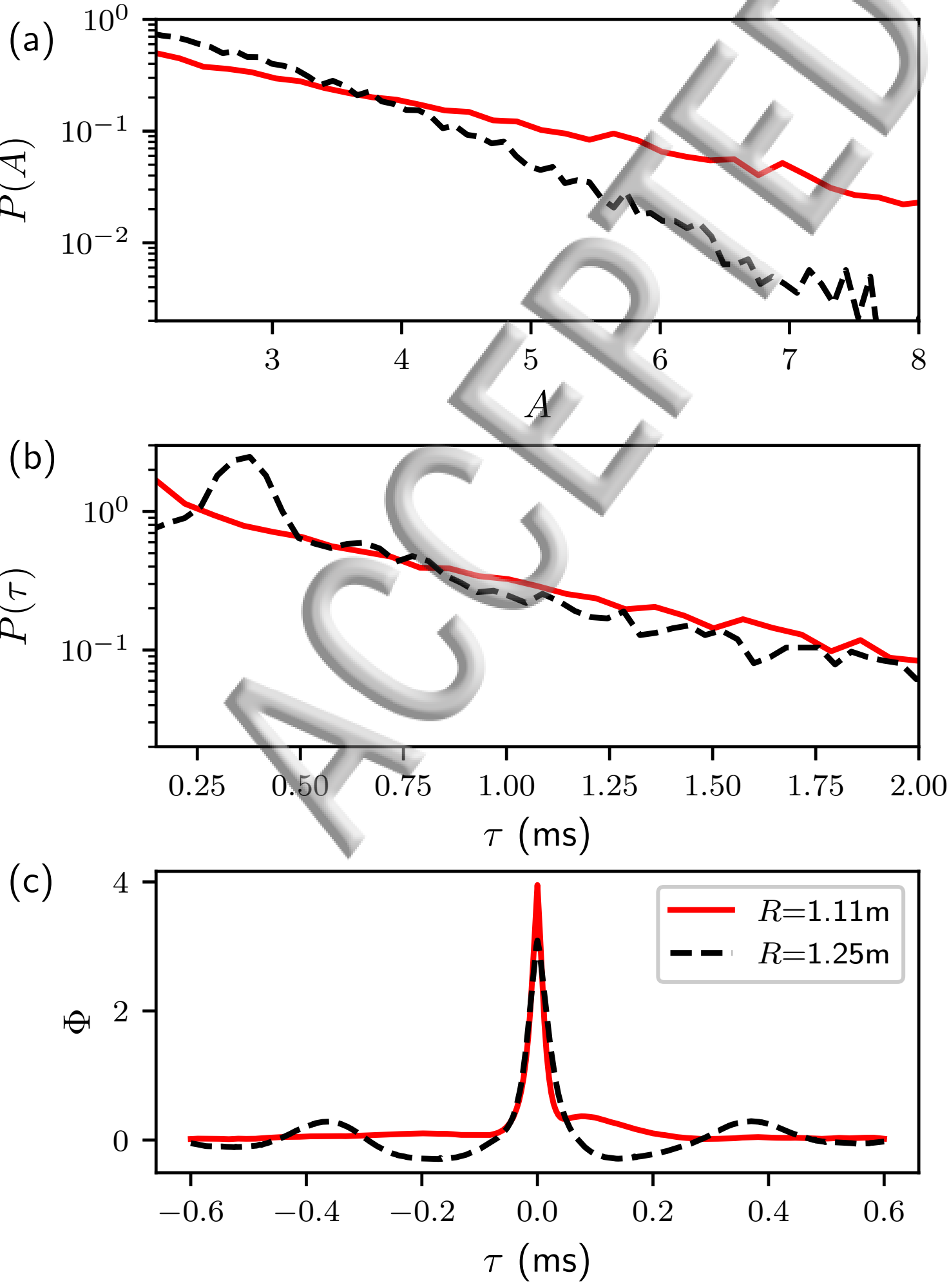
(a)
10^0
10^{-1}
10^{-2}
$P(A)$
3
4
5
6
7
8
A
(b)
10^0
10^{-1}
$P(\tau)$
0.25
0.50
0.75
1.00
1.25
1.50
1.75
2.00
τ (ms)
(c)
4
2
0
Φ
R=1.11m
R=1.25m
−0.6
−0.4
−0.2
0.0
0.2
0.4
0.6
τ (ms)

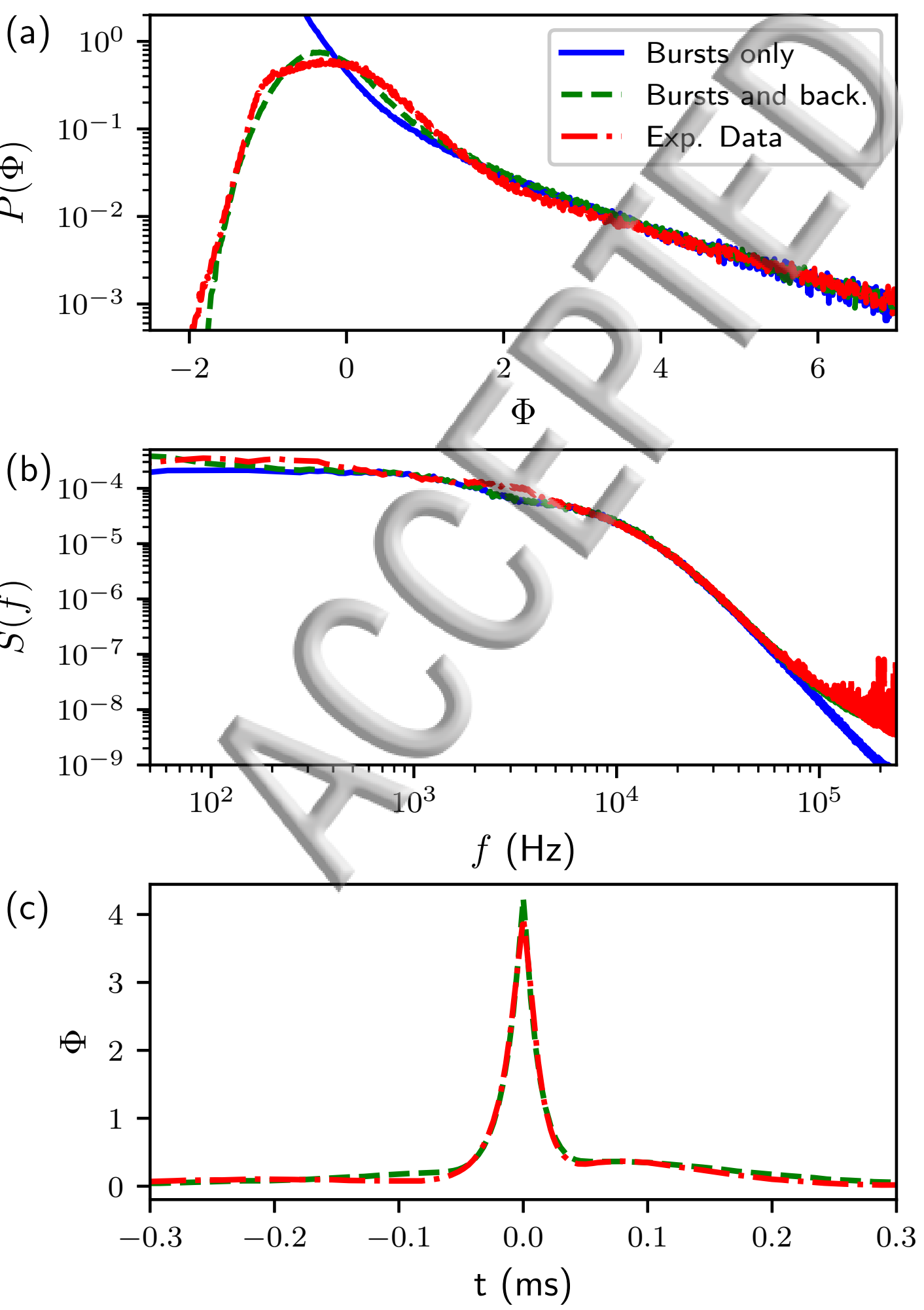
(a)
Bursts only
Bursts and back.
Exp. Data
$P(\Phi)$
Φ
(b)
$S(f)$
f (Hz)
(c)
Φ
t (ms)

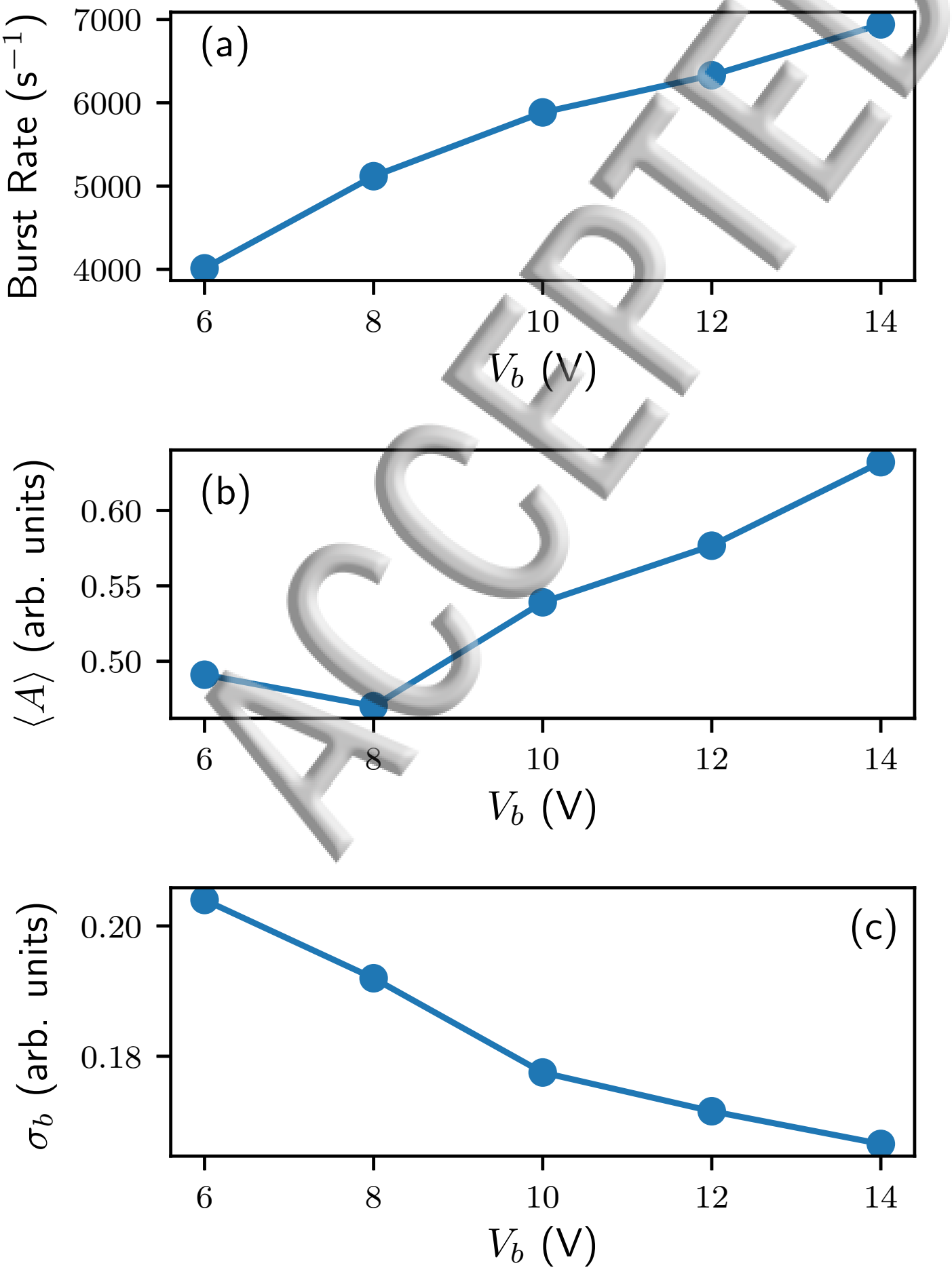
(a)
Burst Rate (s^{-1})
7000
6000
5000
4000
6
8
10
12
14
V_b (V)
(b)
$\langle A \rangle$ (arb. units)
0.60
0.55
0.50
6
8
10
12
14
V_b (V)
(c)
σ_b (arb. units)
0.20
0.18
6
8
10
12
14
V_b (V)

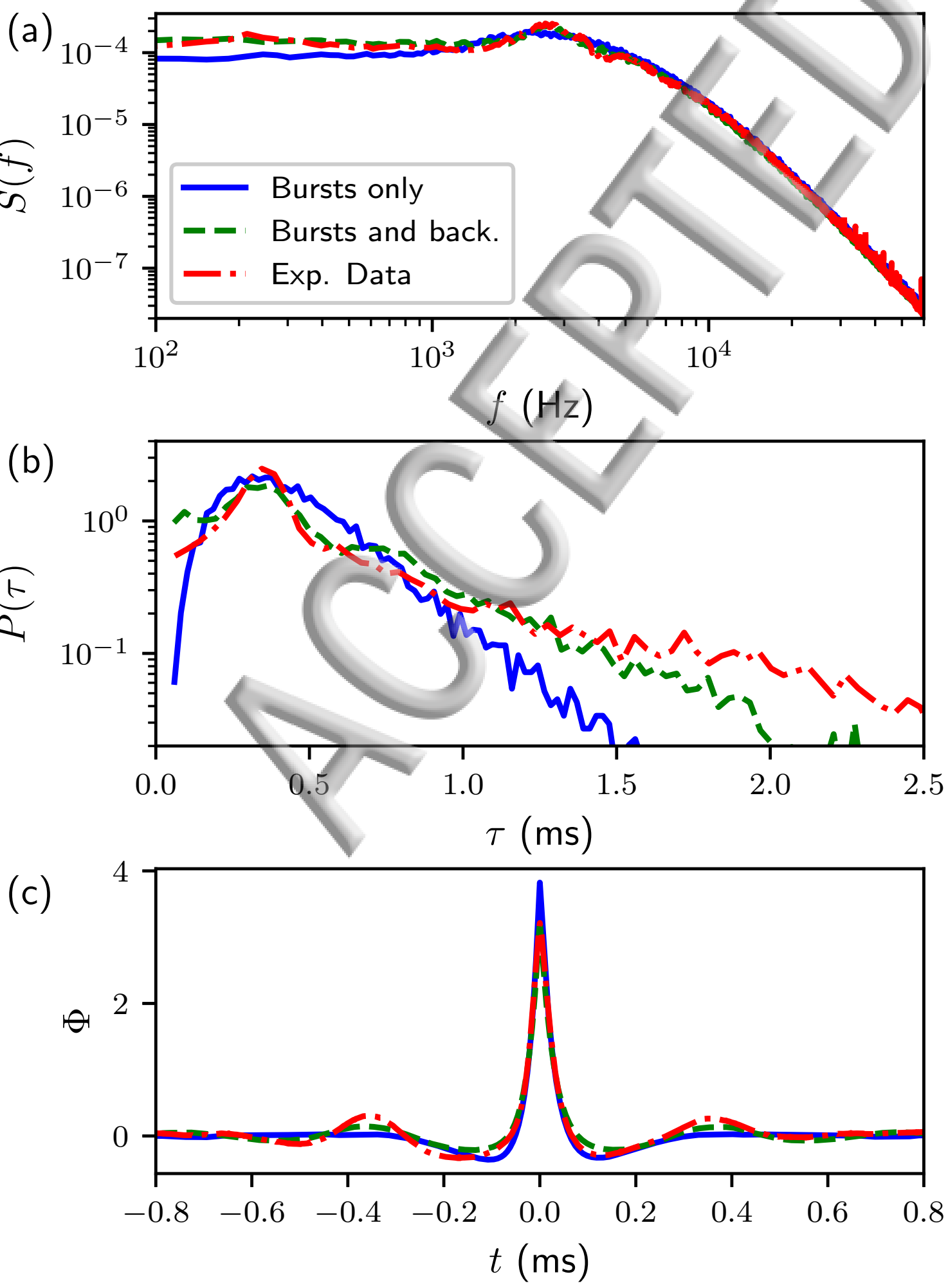
(a)
10^{-4}
10^{-5}
10^{-6}
10^{-7}
$S(f)$
Bursts only
Bursts and back.
Exp. Data
10^2
10^3
10^4
f (Hz)
(b)
10^0
10^{-1}
$P(\tau)$
0.0
0.5
1.0
1.5
2.0
2.5
τ (ms)
(c)
4
2
0
Φ
−0.8
−0.6
−0.4
−0.2
0.0
0.2
0.4
0.6
0.8
t (ms)

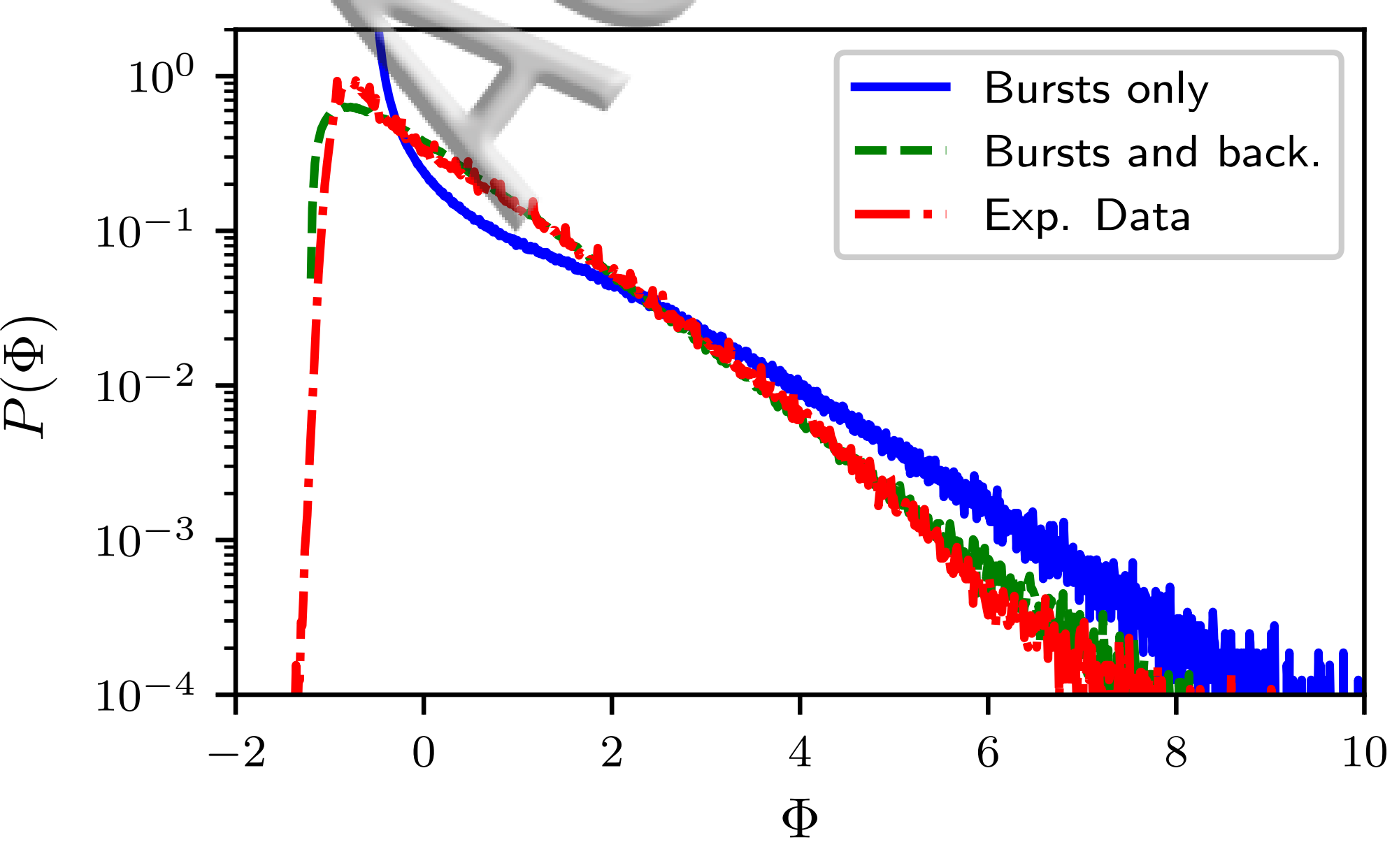
Bursts only
Bursts and back.
Exp. Data
$P(\Phi)$
Φ
10^0
10^{-1}
10^{-2}
10^{-3}
10^{-4}
-2
0
2
4
6
8
10

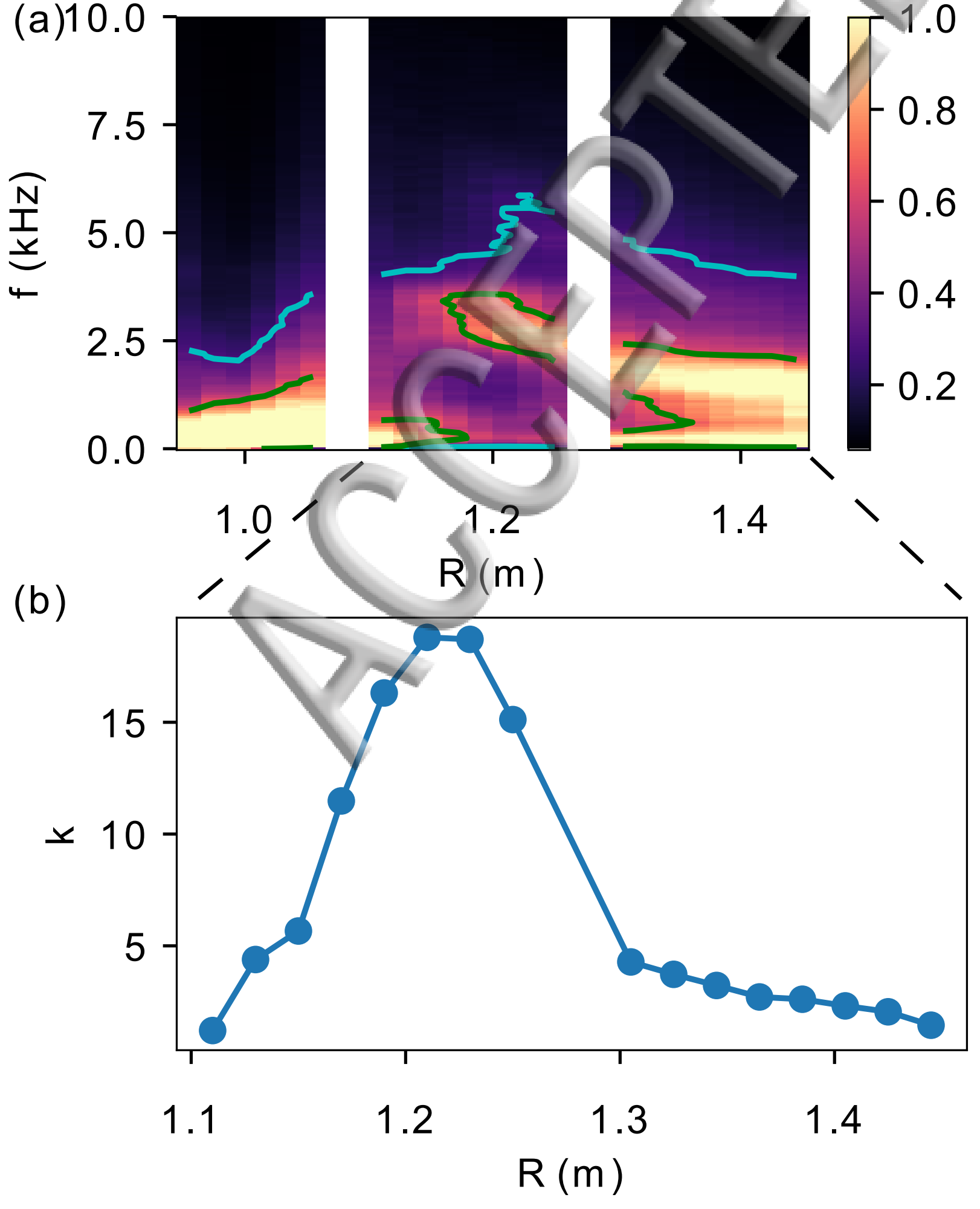
(a)
10.0
7.5
5.0
2.5
0.0
f (kHz)
1.0
0.8
0.6
0.4
0.2
1.0
1.2
1.4
R (m)
(b)
15
10
5
k
1.1
1.2
1.3
1.4
R (m)

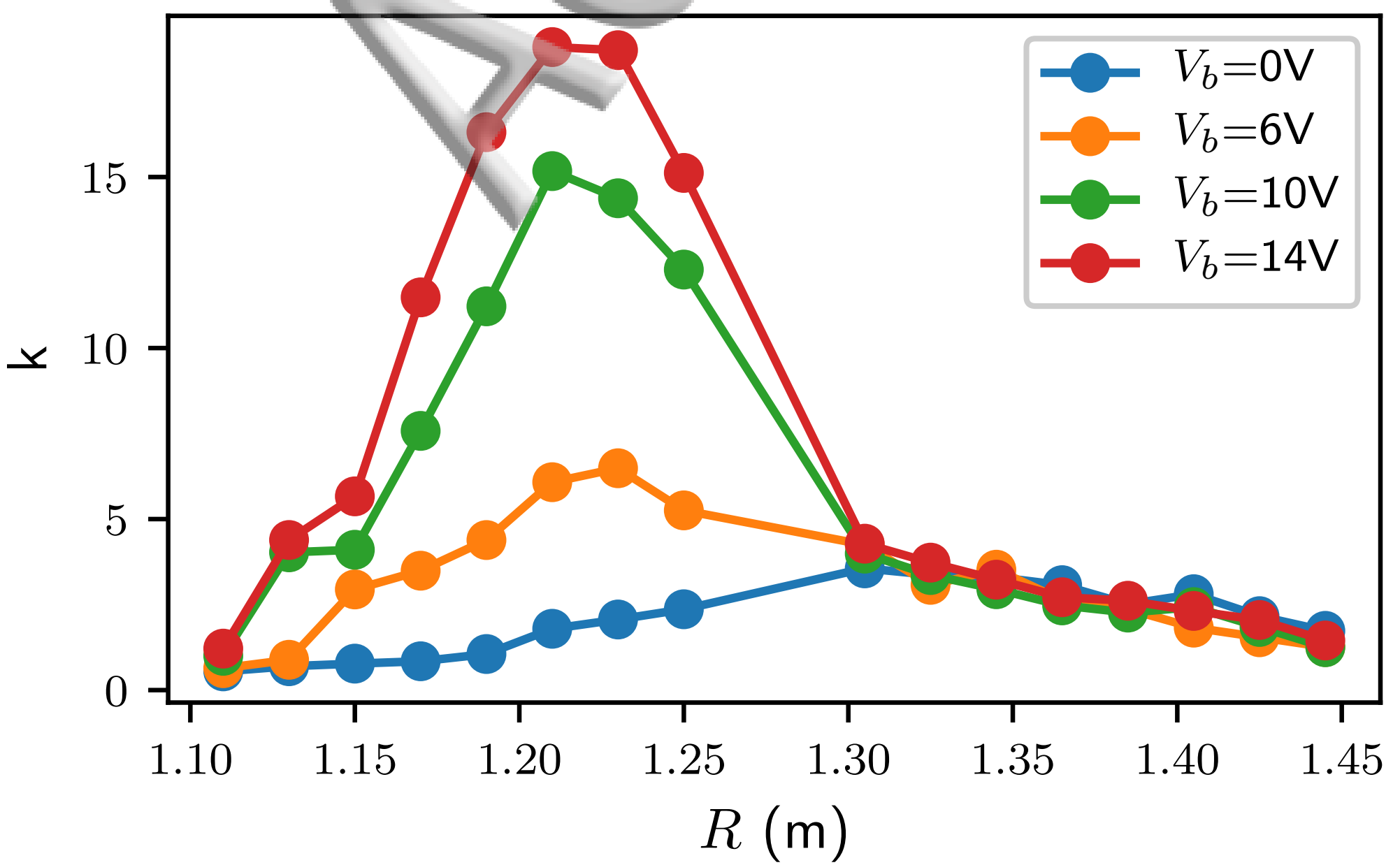
V_b=0V
V_b=6V
V_b=10V
V_b=14V
k
0
5
10
15
1.10
1.15
1.20
1.25
1.30
1.35
1.40
1.45
R (m)